Ineffectiveness of the triplet diffusion correction in the electron transport of disordered systems

Daniel Gnida *

Institute of Low Temperature and Structure Research, Polish Academy of Sciences, Okólna 2, 50-542 Wrocław, Poland

(Received 3 November 2023; revised 25 July 2024; accepted 20 August 2024; published 3 September 2024)

The mystery of the field-independent $T^{1/2}$ behavior of resistivity in single-crystal Th_2CoSi_3 is unraveled through the lens of interacting electrons in disordered systems. Consistent with theoretical predictions, our magnetotransport studies illuminate a scenario where a robust spin-orbit interaction renders the triplet term in the diffusion contribution ineffective. As a consequence, the magnetic field exerts no influence on the diffusion correction, giving sole dominance to weak localization and classical effects in shaping the magnetoresistance. In addition, marginal temperature variation of the weak localization at low temperatures results in the $T^{1/2}$ relation being predominantly dictated by the singlet term in the diffusion correction.

DOI: 10.1103/PhysRevB.110.094201

In the weak disorder limit, electrons in metals sporadically encounter imperfections in the crystal structure, making the classical description of electron transport applicable. However, as the disorder increases, the mean free path of the electrons decreases, so the interference of electron waves scattered by impurities or defects cannot be neglected. As a consequence, the constructive interference of electron waves leads to enhanced coherent backscattering, which in turn, gives rise to the quantum corrections to classical electron transport due to the weak localization (WL) or electron-electron interaction (EEI) effect [1–4]. Typically, these corrections lead to an increase in resistivity with decreasing temperature [5–12], in contrast to what is observed for conventional metals. Notably, however, while the temperature dependence of the WL is governed by the respective dominant inelastic scattering mechanism, the interaction correction (IC), according to the Altshuler-Aronov (AA) theory, in the three-dimensional disordered Fermi liquids follows a $T^{1/2}$ relation [3,4].

Interestingly, this peculiar behavior of resistivity in disordered systems may also be attributed to a non-Fermi-liquid excitation spectrum as a result of the two-channel Kondo (2CK) effect. In this scenario, two degenerate channels of conduction electrons interact identically with tunneling states, functioning as pseudospin variables [13,14]. However, unlike the quasiparticle description within the disordered Fermi liquid approach, the non-Fermi-liquid–based model requires a specific type of disorder that allows the formation of multilevel systems akin to those found in glassy materials [15–17]. Furthermore, the non-Fermi-liquid state can be disrupted either by breaking the degeneracy between the channels or through spontaneous tunneling between different energy levels [13,14]. Consequently, experimental confirmation of the 2CK effect resulting from disorder-induced tunneling states in bulk crystalline disordered compounds is thus extremely challenging [18–20].

The most interesting case is when the anomalous $AT^{1/2}$ increase in resistivity is independent of the magnetic field. Such an experimental observation is considered in the literature as a necessary condition for the nonmagnetic scenario within the 2CK model, although it should be noted that at the same time it does not invalidate the realization of the Altshuler-Aronov model of interacting electrons. Therefore, attempts are made to use other characteristic features of both models to find out which of them is most likely in a particular compound studied [20–28]. One way is to compare the experimental value of the coefficient A with its expected value calculated using the theoretical relation and the numerical material data, but we should be very careful when using this criterion, because the incorrect use of the model with respect to the properties of the studied compound may lead to false conclusions [27,28].

Another method described in the literature to distinguish experimentally between these two mechanisms is based on the search for a logarithmic correction of the resistivity that emerges directly from the non-Fermi-liquid behavior above the Kondo temperature T_K. This characteristic resistivity change has been observed in some ferromagnetic thin films and is considered to be a manifestation of the 2CK effect [23–25]. On the other hand, the absence of a $\log T$ dependence in ferromagnetic Co_2MnAl [29] and Co_2MnGa [30] has been argued, among other reasons, as evidence for EEI corrections. In these compounds, as well as in the superconducting $ZrAs_{1.58}Se_{0.39}$ [27,28], the insensitivity of the $T^{1/2}$ dependence to magnetic field strength is attributed to the vanishingly small electron-electron interaction constant. However, it is important to note that other mechanisms can also lead to the absence of magnetoresistance in the correction of interacting electrons. Therefore, given the controversy and lively discussion surrounding this topic, it is crucial to highlight such examples and experimentally explore the theoretical predictions of the Altshuler-Aronov correction in this field. As an another example of this kind of behavior, in this article we investigate the ineffectiveness of the triplet term as a conducting channel, driven by strong spin-orbit scattering [31]. Surprisingly, this aspect remains relatively unexplored.

*Contact author: d.gnida@intibs.pl

Previous experimental research has mainly focused on spin relaxation from the perspective of the WL effect [32–36]. Only a few investigations have addressed this issue, suggesting that the triplet contribution vanishes when the spin-orbit relaxation rate falls in the range of 10^{-12} to 10^{-13} s^{-1}, although the field independence of the IC has not been directly addressed [8,37].

To gain a better understanding of this phenomenon, we have carried out a detailed magnetotransport study of disordered Th_2CoSi_3. It is a nonmagnetic representative of the AlB_2-type structure compound with the general formula M_2TSi_3, where T = transition element and M = La, Ce, U [38,39]. Similar to many of these materials [40–44], Th_2CoSi_3 exhibits an unusual increase in resistivity at low temperatures. However, its field independence makes it unique among other M_2TSi_3 compounds. This, combined with the presence of strong spin-orbit interaction in this material, makes it an excellent candidate for investigating how electron spin relaxation affects the IC and provides an opportunity to check on previous experimental findings and hypotheses.

A single crystal of Th_2CoSi_3 was grown by the Czochralski pulling technique in a tetra-arc furnace under an ultrapure argon atmosphere. The orientation and structure of the crystal were determined by x-ray diffraction. The lattice parameters derived from the XRD of powder samples give $a = 4.0338(1)$ Å, $c = 4.1872(1)$ Å, which are very close to those previously determined [38,39]. Magnetic properties, heat capacity, and resistivity were investigated using Quantum Design MPMS and PPMS instruments. Two oriented single-crystalline samples with dimensions of $0.8 \times 0.7 \times 3.2$ mm and $0.5 \times 0.6 \times 2.8$ mm were used for electron transport measurements. Electrical connections were made using 50 μm silver wire and silver paint. The four-point AC resistivity measurements were performed with the current either parallel or perpendicular to the c axis of the hexagonal unit cell in magnetic fields up to 9 T and in the temperature range of 2–300 K. To enhance measurement quality, external Lake Shore AC 370 Resistance Bridges were employed.

A preliminary characterization of the Th_2CoSi_3 single-crystalline samples was carried out by studying the thermodynamic properties. As shown in Fig. 1(a), the heat capacity shows no phase transitions over the whole temperature range studied. At high temperatures its magnitude approaches the Dulong-Petit limit, i.e., $3n_aR \simeq 150\,\mathrm{J\,mol^{-1}\,K^{-1}}$, where n_a is the number of atoms per formula unit and R is the gas constant. In turn, as shown in Fig. 1(b), the ratio of specific heat to temperature is a linear function of T^2 below 7 K. Employing the Debye model approximation, the obtained electronic specific heat coefficient γ and Debye temperature Θ_D were determined to be $\gamma = 8.5\,\mathrm{mJ\,mol^{-1}\,K^{-2}}$ and $\Theta_D = 370$ K, respectively. The γ value is similar to that obtained for La_2NiSi_3 ($\gamma = 11\,\mathrm{mJ\,mol^{-1}\,K^{-2}}$) [43]. This may suggest that the slightly enhanced γ coefficient of the nonmagnetic representatives of the AlB_2-type structure compared to the simple s-type metals is most likely due to the contribution of the d electrons to the total density of states.

Figure 1(c) shows the temperature dependence of the magnetic susceptibility (χ) of Th_2CoSi_3 measured with the magnetic field directed along the c axis and the a axis of the hexagonal unit cell. Irrespective of the sample's orientation,

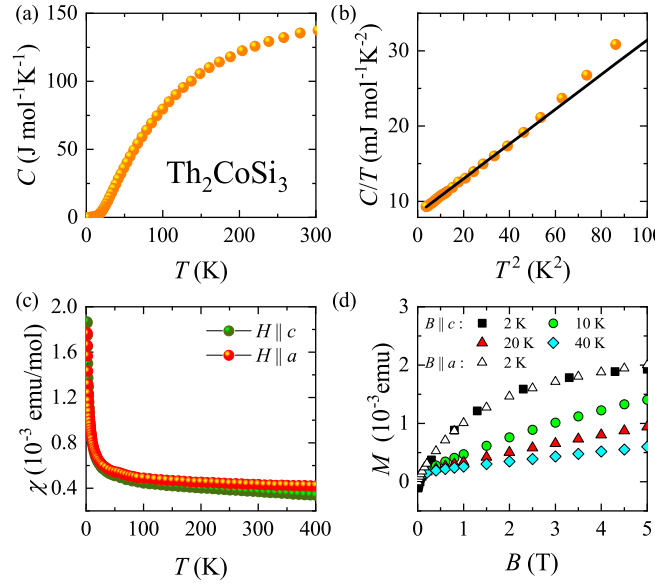

FIG. 1. (a) Heat capacity, C, of Th_2CoSi_3 vs temperature. (b) C/T vs T^2. The solid line is a Debye model fit to the low-temperature heat capacity data. (c) Magnetic susceptibility of Th_2CoSi_3 as a function of temperature measured with the magnetic field oriented along crystallographic a and c axes. (d) Magnetization of Th_2CoSi_3 for different orientations of magnetic field and temperatures.

the χ changes with temperature in a similar manner. As evident from the plot, it remains almost constant between 400 and 50 K, indicating Pauli paramagnetic behavior. However, below about 50 K the χ increases rapidly, probably due to the presence of paramagnetic impurities. The magnetization (M) measurement shown in Fig. 1(d) supports this interpretation. The $M(B)$ observed at 2 K has a Brillouin-like shape which is attributed to the paramagnetic impurities. However, with increasing temperature its contribution to the total M decreases in favor of a linear Pauli paramagnetic term.

Figures 2(a) and 2(b) show the temperature dependence of the resistivity of Th_2CoSi_3 measured along the main crystallographic directions. As can be seen, both ρ_a and ρ_c are very typical of disordered metals. Although in the broad temperature range measured, ρ_a and ρ_c predominantly decrease with decreasing temperature, the residual resistivity ratio takes a value close to unity in both cases. This is mainly due to the significantly increased residual resistivity (ρ_0) compared to clean metals, indicating that elastic scattering at crystal structure imperfections is the dominant scattering mechanism in this compound. Another characteristic of disordered metals observed in Th_2CoSi_3 is the low-temperature increase in resistivity, which manifests itself below the minimum at $T_{min} = 20$ K. Significantly, as shown in Figs. 2(c) and 2(d), this additional contribution to resistivity is proportional below $T^* \simeq 10$ K to the $T^{1/2}$ relation, regardless of the crystallographic direction. Employing least-squares fitting of the experimental data below 10 K to the simple formula $\Delta\rho_i(T) = \rho_i(T) - \rho_{0i} = A_iT^{1/2}$, where i represents either a or c as the crystallographic direction, we obtained the following parameters: $\rho_{0c} = 250\,\mu\Omega\,\mathrm{cm}$, $A_c = -0.17\,\mu\Omega\,\mathrm{cm\,T^{-1/2}}$, and $\rho_{0a} = 326\,\mu\Omega\,\mathrm{cm}$, $A_a = -0.22\,\mu\Omega\,\mathrm{cm\,T^{-1/2}}$.

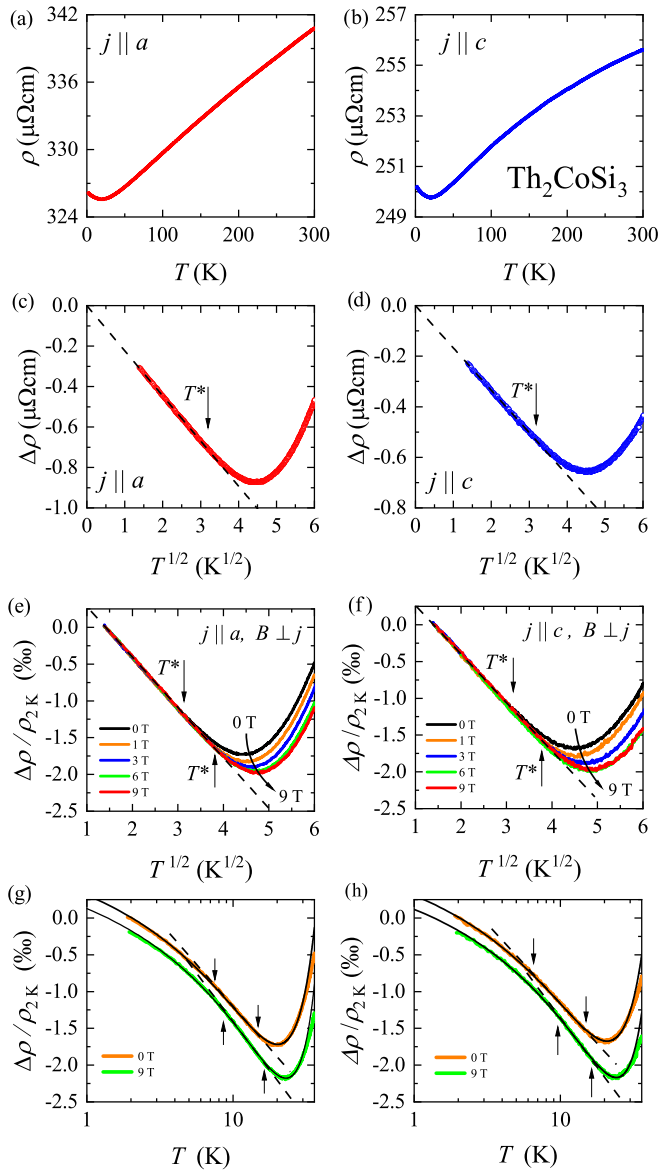

FIG. 2. [(a), (b)] The resistivity ρ_a and ρ_c of Th_2CoSi_3 measured along the crystallographic axes a and c, respectively. [(c), (d)] The ρ_a and ρ_c vs $T^{1/2}$. [(e), (f)] Effect of the magnetic field on the quantum correction to the resistivity. The dashed lines represent the fitted relation $T^{1/2}$ to the experimental data. The arrows indicate the onset of the $T^{1/2}$ relation in $\rho(T)$ for $B = 0$ and 9 T. [(g), (h)] The resistivity data for $B = 0$ T and 9 T, plotted on a $\log T$ scale. The $B = 9$ T data are shifted for clarity. The dashed lines represent the $\log T$ dependence, while the arrows indicate the T range over which it holds. The solid lines represent the fitted curves, which consist of two components of opposite sign: $-T^{1/2}$ and T^a.

Figures 2(e) and 2(f) show the effect of a magnetic field on the $AT^{1/2}$ resistivity correction. These figures clearly show that as the magnetic field strength increases, $T_{\min}$ and T^* shift toward higher temperatures, while the A coefficient remains unaffected. The absence of a visible magnetic field effect on the resistivity upturn rules out an interpretation based on the magnetic single-ion Kondo effect. The magnetic-field-induced increase of T^*, which in the 2CK model can be associated with the Kondo temperature T_K, suggests that this scenario is also not relevant in the studied compound. Admittedly, as shown in Figs. 2(g) and 2(h), there is a small temperature interval in $\rho(T)$ that can be described by the $a \log T$ relation, but the a coefficient changes when the magnetic field is increased to 9 T. These experimental observations are not typical for the nonmagnetic two-level system (TLS) Kondo model, as it would imply that T_K varies with the magnetic field. The change in the a factor in this case may indicate that this narrow temperature range is governed by a power law, since $a \log T = \log T^a$. In fact, if we consider that $\rho(T)$ consists of two terms with opposite signs: $-T^{1/2}$ and T^a, then we can obtain a very good agreement with the experimental data, as shown by a solid line in Figs. 2(g) and 2(h). This additional contribution to $\rho(T)$, which is proportional to T^a, is most likely due to the superposition of the classical and WL effects in electron transport [see Figs. 5(b) and 5(c)].

Since the explanation of the low-T resistivity in Th_2CoSi_3 within the 2CK effect scenario is unlikely, the results are further analyzed in terms of EEI and WL effects. The clear $T^{1/2}$ dependence of resistivity below T^* suggests that the interaction between particles in the diffusion channel is the dominant contribution in this temperature range. The resulting correction to the conductivity can be described by the equation [3,4,45,46]

$$\Delta\sigma_{\mu\mu} = \frac{0.915e^2}{4\pi^2\hbar^{3/2}}\left(\frac{4}{3} - \frac{3}{2}\lambda\right)\frac{D_{\mu\mu}k_B^{1/2}T^{1/2}}{(D_{xx}D_{yy}D_{zz})^{1/2}}, \qquad (1)$$

where $D_{\mu\mu}$ represents the principal values of the diffusion coefficient tensor and λ denotes the electron screening parameter. The bracketed terms correspond to the singlet and triplet diffusion contributions, respectively. However, as will be shown from the magnetoresistivity data, Th_2CoSi_3 exhibits significant conduction electron spin relaxation, rendering the triplet contribution ineffective in this scenario. Consequently, the IC is solely determined by the singlet diffusion channel. Furthermore, assuming that the diffusion tensor can be represented by an ellipsoid of revolution with the principal long axis aligned with the crystallographic c direction, i.e., $D_a = D_{xx} = D_{yy}$ and $D_c = D_{zz}$, we can easily derive, using the Einstein relation, that the IC takes the following form depending on the crystallographic direction [3,4,46,47]:

$$\Delta\rho_i = -A_x\rho_i^2\frac{D_c^{1/2}}{D_i}T^{1/2}, \qquad (2)$$

where A_x is a numerical factor defined by the constants in Eq. (1). These equations accurately represent the experimental results using the following diffusion coefficients: $D_a = 1.32\ \mathrm{cm^2\,s^{-1}}$ and $D_c = 1.68\ \mathrm{cm^2\,s^{-1}}$.

The possible effect of WL on the low-T resistivity of Th_2CoSi_3 was verified by magnetoresistance (MR) measurements. The results of MR and their analysis are shown in Figs. 3 and 4. The total MR between 0 and 9 T can be described as a sum of two components: the WL (MR_{wl}) and the classical (MR_{cl}). The MR_{cl} contribution can be approximated by the relation $MR_{cl} = (\omega_c\tau)^2 = a_nB^2$, where ω_c and τ are cyclotron frequency and relaxation time, respectively. In turn, MR_{wl} can be determined by a formula that takes into account

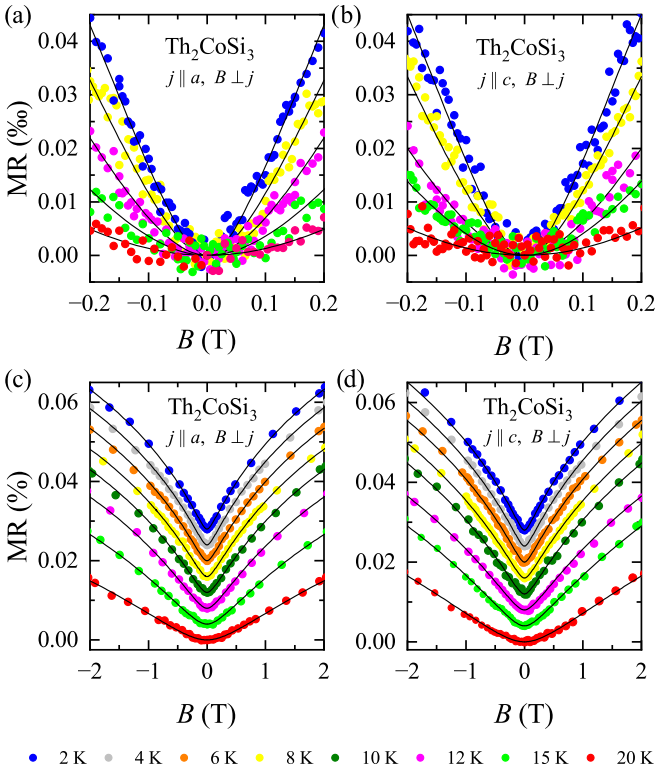

FIG. 3. Transverse MR of Th_2CoSi_3 between –0.2 and 0.2 T [(a), (b)] and –2 to 2 T [(c), (d)]. The solid lines represent the fit using Eq. (3). In both ranges the values of the fit parameters are exactly the same. In the upper panel the MR data at 4, 6, and 10 K have been omitted, while in the lower panel the corresponding curves have been shifted for clarity.

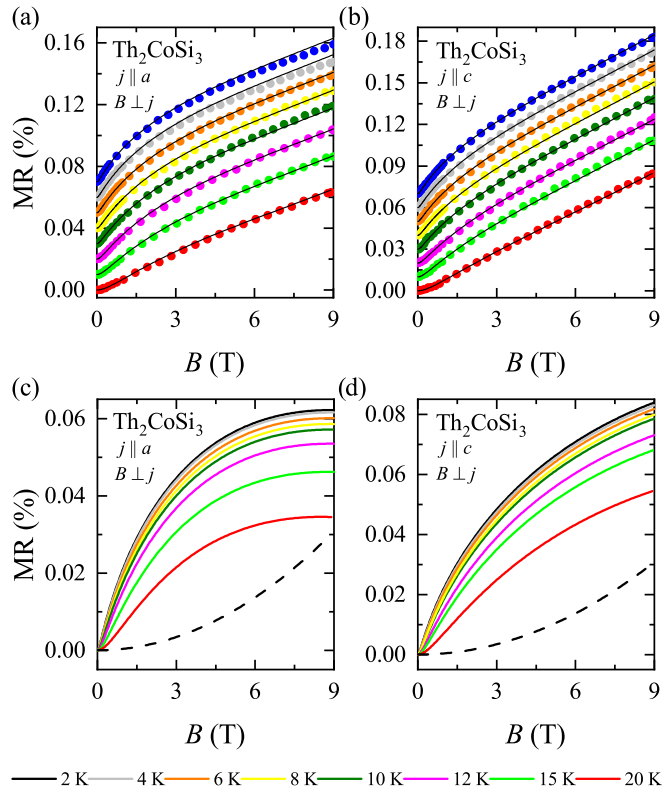

FIG. 4. [(a), (b)] Transverse MR of Th_2CoSi_3 between 0 and 9 T. The solid lines represent the sum of the WL [Eq. (3)] and the classical MR. The corresponding curves have been shifted for clarity. [(c), (d)] Separated MR_{wl} (solid lines) and MR_{cl} (dashed lines) contributions.

the spin-orbit interaction and anisotropic diffusion [4]:

$$\Delta\sigma_{\mu\mu} = \frac{A_\omega e^2}{2\pi^2\hbar}\left(\frac{eB}{\hbar}\right)^{1/2}\left[\frac{1}{2}f\left(\frac{B}{B_\varphi}\right) - \frac{3}{2}f\left(\frac{B}{B_2}\right)\right]. \quad (3)$$

In this equation, A_ω, which is a parameter resulting from the anisotropic diffusion coefficient, is defined as follows: $A_\omega = \frac{D_{\mu\mu}}{D_x}(\frac{D_\omega}{D_x})^{1/2}$, where $D_x = [\det D_{\mu\mu}]^{1/3}$ and $D_\omega^2 = D_\perp(D_\parallel \sin^2\theta + D_\perp \cos^2\theta)$. Here, D_ω represents the "cyclotron" diffusion coefficient, and θ is the angle between the axis of the ellipsoid and the magnetic field induction [4]. Furthermore, the function $f(\frac{B}{B_j})$ corresponds to the Kawabata function [48], where the characteristic fields B_φ and B_2 are expressed as $B_\varphi = B_i + 2B_s$ and $B_2 = B_i + 2B_s/3 + 4B_{so}/3 = B_\varphi + 4B^*_{so}/3$. The characteristic field B_j is related to the characteristic scattering time τ_j by the relation $B_j = \hbar/4eD_\omega\tau_j$, where $j = i, so, s$ refer to the inelastic, spin-orbit, and T-independent spin-spin scattering times, respectively.

From the analysis, it is clear that in the magnetic field range up to 2 T, the MR data can be fully described using only the WL contribution given by Eq. (3). As shown in Figs. 3(a)–3(d), the fits reproduce the experimental data very well, both in the initial field region and in the extended scale up to 2 T, with the parameters τ_φ^{-1}, τ_s^{-1}, τ_{so}^{-1}, whose values are given in Fig. 5(a) and Table I. On the other hand, as shown in Figs. 4(a) and 4(b), it is necessary to consider also the classical MR in order to obtain agreement with the experimental results in stronger fields. Remarkably, it was found that the MR in the whole field range can be described by a sum of MR_{wl} and MR_{cl} using the fixed values of the fitting parameters obtained from the low-field range and the coefficients a_n equal to 0.0037% T^{-2} and 0.0038% T^{-2} for the a and c axes, respectively. It is also worth noting that MR_{cl} is proportional

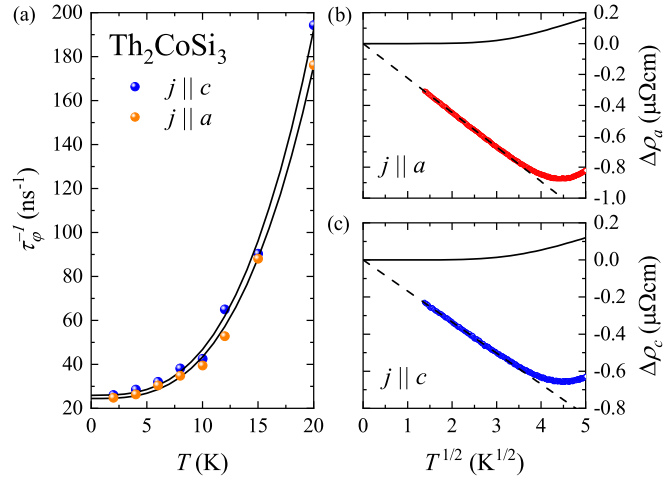

FIG. 5. (a) Dephasing rate in Th_2CoSi_3 determined from MR analysis. The solid lines represent the fitted relation: $\tau_\varphi^{-1} = 2\tau_s^{-1} + a_i T^3$. [(b), (c)] The low-$T$ region of ρ_a and ρ_c. The dashed and solid lines represent the EEI and WL contributions, respectively.

TABLE I. The a_i factor and the characteristic relaxation rates τ_j^{-1} determined from the MR analysis.

Axis	a_i (s^{-1} K^{-3})	τ_i^{-1} (10 K) (s^{-1})	τ_s^{-1} (s^{-1})	τ_{so}^{-1} (s^{-1})
a	1.89×10^7	1.89×10^{10}	1.22×10^{10}	2.00×10^{12}
c	2.08×10^7	2.08×10^{10}	1.30×10^{10}	4.52×10^{12}

to B^2, as is MR_{wl} in the low-field limit, but it is much smaller than MR_{wl}, so omitting it does not violate the fitting procedure below 2 T. For example, as shown in Figs. 4(c) and 4(d), which presents the MR_{wl} and MR_{cl} contributions, even at a field of 2 T, MR_{cl} is only 0.0015%, which is 10 times smaller than MR_{wl} at 20 K.

The $\tau_\varphi^{-1}(T)$ obtained from the MR analysis is shown in Fig. 5(a). As we can observe, τ_φ^{-1} decreases rapidly with decreasing temperature, but below 10 K the rate of decrease slows down with a clear tendency to saturation. Over the studied temperature range, τ_φ^{-1} can be described by a relation $\tau_\varphi^{-1} = 2\tau_s^{-1} + a_i T^n$. The T-dependent term represents the dephasing rate due to either electron-phonon or electron-electron scattering. While in a dirty limit for the latter mechanism $n = 3/2$, for the former n adopts value between 2 and 4, depending on the different phonon modes involved in the scattering process [49–51]. In our case one can obtain a good fit using the values of a_i given are Table I and $n = 3$. Thus, it shows that the temperature variation of the τ_φ^{-1} in Th_2CoSi_3 is dominated by the electron-phonon scattering. Conventionally, it is believed that since the inelastic scattering of the electron with other electrons or phonons vanishes as T approaches zero, the τ_φ^{-1} should also vanish. However, it turns out that in many systems the τ_φ^{-1} tends to finite value [51–53].

Several mechanisms have been proposed to explain the saturation of τ_φ^{-1}, including zero-point motion, high-frequency external noise, spin-spin scattering, electron scattering from TLS impurities, and others [51,52,54–56]. Although the search for the microscopic origins of zero-T dephasing has been the subject of extensive theoretical and experimental investigation, the problem appears to remain unsolved [51]. Among the existing scenarios, spin-spin scattering is often proposed, because the magnetic impurity-free samples are usually difficult to obtain [8,57,58]. It seems that this scenario can be considered as most likely in Th_2CoSi_3, since the magnetic susceptibility clearly shows the presence of paramagnetic admixtures.

It is also worth noting that τ_s^{-1} and τ_i^{-1} are comparable in size below about 10 K. To see what effect this might have on the WL correction, calculations of its magnitude were made using the relationship [4,59]

$$\Delta\sigma_{\mu\mu} = \frac{e^2}{2\pi^2\hbar}\frac{D_{\mu\mu}}{[\det D_{\mu\mu}]^{1/2}}\left(3\sqrt{\frac{1}{\tau_{so}}+\frac{1}{4\tau_\varphi}}-\sqrt{\frac{1}{4\tau_\varphi}}\right). \quad (4)$$

As evident from the Figs. 5(b) and 5(c), the calculated WL contribution to $\rho(T)$ is significantly smaller than that of the IC. It is worth also noticing that τ_{so} is much shorter then τ_φ even at 20 K, which places the investigated Th_2CoSi_3 in the antilocalization regime. This causes the WL correction to increase with increasing temperature; however, the rate of increase is relatively modest due to the most likely substantial contribution of the spin-pin scattering term to the dephasing process.

In conclusion, the magnetotransport results of Th_2CoSi_3 presented in this study validate the scenario within the Altshuler-Aronov theory in which the triplet diffusion channel does not play a role in the IC of disordered conducting systems under strong spin-orbit interaction. As a consequence, the IC of the conductivity of Th_2CoSi_3 remains unaffected by magnetic field. Remarkably, the small magnitude of the WL correction compared to the dominant IC and its saturation below 10 K ensures that the WL effect does not violate the $T^{1/2}$ dependence in the studied Th_2CoSi_3.

The author thanks M. Daszkiewicz and M. Szlawska for checking the crystal structure and crystallographic orientation of the studied samples.

[1] E. Abrahams, P. W. Anderson, D. C. Licciardello, and T. V. Ramakrishnan, Scaling theory of localization: Absence of quantum diffusion in two dimensions, Phys. Rev. Lett. **42**, 673 (1979).

[2] B. L. Altshuler, A. G. Aronov, and P. A. Lee, Interaction effects in disordered Fermi systems in two dimensions, Phys. Rev. Lett. **44**, 1288 (1980).

[3] B. L. Altshuler and A. G. Aronov, Contribution to the theory of disordered metals in strongly doped semiconductors, Zh. Eksp. Teor. Fiz. **77**, 2028 (1979) [Sov. Phys. JETP **50**, 968 (1979)].

[4] B. L. Altshuler and A. G. Aronov, *Electron-Electron Interactions in Disordered Systems* (Elsevier, Amsterdam, 1985).

[5] C. Y. Wu, W. B. Jian, and J. J. Lin, Phonon-induced electron-electron interaction in disordered superconductors, Phys. Rev. B **52**, 15479 (1995).

[6] J. J. Lin and C. Y. Wu, Electron-electron interaction and weak-localization effects in Ti-Al alloys, Phys. Rev. B **48**, 5021 (1993).

[7] R. W. Cochrane and J. O. Strom-Olsen, Scaling behavior in amorphous and disordered metals, Phys. Rev. B **29**, 1088 (1984).

[8] A. Sahnoune, J. O. Ström-Olsen, and H. E. Fischer, Influence of spin-orbit scattering on the magnetoresistance due to enhanced electron-electron interactions, Phys. Rev. B **46**, 10035 (1992).

[9] M. Olivier, J. O. Strom-Olsen, Z. Altounian, R. W. Cochrane, and M. Trudeau, Weak-localization and Coulombic interaction effects in the low-temperature resistivity and magnetoresistivity of Y-Al metallic glasses, Phys. Rev. B **33**, 2799 (1986).

[10] S. Dhara, R. R. Chowdhury, and B. Bandyopadhyay, Observation of resistivity minimum at low temperature in Co_xCu_{1-x} ($x \sim 0.17$–0.76) nanostructured granular alloys, Phys. Rev. B **93**, 214413 (2016).

[11] W. B. Jian, C. Y. Wu, Y. L. Chuang, and J. J. Lin, Electron-electron interaction and normal-state transport in superconducting Ti-(Sn,Ge) alloys, Phys. Rev. B **54**, 4289 (1996).

[12] K. Ciesielski, L. C. Gomes, G. A. Rome, E. A. Bensen, J. M. Adamczyk, D. Kaczorowski, E. Ertekin, and E. S. Toberer,

Structural defects in compounds ZnXSb(X = Cr, Mn, Fe): Origin of disorder and its relationship with electronic properties, Phys. Rev. Mater. **6**, 063602 (2022).
[13] D. Cox and A. Zawadowski, Exotic Kondo effects in metals: Magnetic ions in a crystalline electric field and tunneling centers, Adv. Phys. **47(5)**, 599 (1998).
[14] D. L. Cox and M. Jarrell, The two-channel Kondo route to non-Fermi-liquid metals, J. Phys.: Condens. Matter **8**, 9825 (1996).
[15] R. B. Stephens, Low-temperature specific heat and thermal conductivity of noncrystalline dielectric solids, Phys. Rev. B **8**, 2896 (1973).
[16] R. C. Zeller and R. O. Pohl, Thermal conductivity and specific heat of noncrystalline solids, Phys. Rev. B **4**, 2029 (1971).
[17] R. W. Cochrane, R. Harris, J. O. Ström-Olson, and M. J. Zuckermann, Structural manifestations in amorphous alloys: Resistance minima, Phys. Rev. Lett. **35**, 676 (1975).
[18] I. L. Aleiner, B. L. Altshuler, Y. M. Galperin, and T. A. Shutenko, Kondo temperature for the two-channel Kondo models of tunneling centers, Phys. Rev. Lett. **86**, 2629 (2001).
[19] L. Borda, A. Zawadowski, and G. Zaránd, Orbital Kondo behavior from dynamical structural defects, Phys. Rev. B **68**, 045114 (2003).
[20] S. Kirchner, Two-channel Kondo physics: From engineered structures to quantum materials realizations, Adv. Quantum Technol. **3**, 1900128 (2020).
[21] T. Cichorek, A. Sanchez, P. Gegenwart, F. Weickert, A. Wojakowski, Z. Henkie, G. Auffermann, S. Paschen, R. Kniep, and F. Steglich, Two-channel Kondo effect in glasslike ThAsSe, Phys. Rev. Lett. **94**, 236603 (2005).
[22] T. Cichorek, L. Bochenek, M. Schmidt, A. Czulucki, G. Auffermann, R. Kniep, R. Niewa, F. Steglich, and S. Kirchner, Two-channel Kondo physics due to As vacancies in the layered compound $ZrAs_{1.58}Se_{0.39}$, Phys. Rev. Lett. **117**, 106601 (2016).
[23] S. Gupta, R. Sachan, and J. Narayan, Emergence of orbital two-channel Kondo effect in epitaxial TiN thin films, Solid State Commun. **341**, 114547 (2022).
[24] L. J. Zhu, S. H. Nie, P. Xiong, P. Schlottmann, and J. H. Zhao, Orbital two-channel Kondo effect in epitaxial ferromagnetic $L1_0$-MnAl films, Nat. Commun. **7**, 10817 (2016).
[25] L. Zhu, G. Woltersdorf, and J. Zhao, Observation of orbital two-channel Kondo effect in a ferromagnetic $L1_0$-MnGa film, Sci. Rep. **6**, 34549 (2016).
[26] S.-S. Yeh, T.-K. Su, A.-S. Lien, F. Zamani, J. Kroha, C.-C. Liao, S. Kirchner, and J.-J. Lin, Oxygen vacancy-driven orbital multichannel Kondo effect in Dirac nodal line metals IrO_2 and RuO_2, Nat. Commun. **11**, 4749 (2020).
[27] D. Gnida, Comment on "Two-channel Kondo physics due to As vacancies in the layered compound $ZrAs_{1.58}Se_{0.39}$," Phys. Rev. Lett. **118**, 259701 (2017).
[28] D. Gnida, Origin of the $-|A|T^{1/2}$ term in the resistivity of disordered $ZrAs_{1.58}Se_{0.39}$, Phys. Rev. B **97**, 134201 (2018).
[29] L. J. Zhu and J. H. Zhao, Anomalous resistivity upturn in epitaxial $L2_1$-Co_2MnAl films, Sci. Rep. **7**, 42931 (2017).
[30] S. Tong, X. Zhao, D. Wei, and J. Zhao, Low-temperature resistivity anomaly and weak spin disorder in Co_2MnGa epitaxial thin films, Phys. Rev. B **101**, 184434 (2020).
[31] Y. Lyanda-Geller, Quantum interference and electron-electron interactions at strong spin-orbit coupling in disordered systems, Phys. Rev. Lett. **80**, 4273 (1998).
[32] G. Bergman, Influence of spin-orbit coupling on weak localization, Phys. Rev. Lett. **48**, 1046 (1982).
[33] G. Bergmann, Consistent temperature and field dependence in weak localization, Phys. Rev. B **28**, 515 (1983).
[34] C. Y. Wu and J. J. Lin, Weak-localization and Maki-Thompson superconducting fluctuation effects in crystalline disordered Ti-Al-(Sn,Co) alloys at $T > T_c$, Phys. Rev. B **50**, 385 (1994).
[35] J. J. Lin and N. Giordano, Localization and electron-electron interaction effects in thin Au-Pd films and wires, Phys. Rev. B **35**, 545 (1987).
[36] A. Sahnoune and J. O. Strom-Olsen, Weak localization and enhanced electron-electron interaction in amorphous $Ca_{70}(Mg, Al)_{30}$, Phys. Rev. B **39**, 7561 (1989).
[37] J. Lin, S. Hsu, J. Lue, and P. Sheng, Spin–orbit scattering effect on electron–electron interactions in disordered metals, J. Phys. Chem. Solids **62**, 1813 (2001).
[38] W. X. Zhong, W. L. Ng, B. Chevalier, J. Etourneau, and P. Hagenmuller, Structural and electrical properties of new silicides: $ThCo_xSi_{2-x}$ ($0 \leqslant x \leqslant 1$) and ThTSi (T = Ni, Pt), Mater. Res. Bull. **20**, 1229 (1985).
[39] J. H. Albering, R. Pöttgen, W. Jeitschko, R.-D. Hoffmann, B. Chevalier, and J. Etourneau, On the order and disorder of the transition metal (T) and silicon atoms in ternary thorium transition metal silicides of the compositions Th_2TSi_3 and ThTSi, J. Alloys Compd. **206**, 133 (1994).
[40] M. Szlawska, D. Gnida, and D. Kaczorowski, Magnetic and electrical transport behavior in the crystallographically disordered compound U_2CoSi_3, Phys. Rev. B **84**, 134410 (2011).
[41] D. Gnida, M. Szlawska, P. Wiśniewski, and D. Kaczorowski, Quantum interference in disordered ferromagnet U_2NiSi_3, Acta Phys. Pol. A **127**, 451 (2015).
[42] M. Szlawska, D. Kaczorowski, and M. Reehuis, Experimental study of magnetic ordering in single-crystalline U_2NiSi_3, Phys. Rev. B **81**, 094423 (2010).
[43] D. Gnida, M. Szlawska, P. Swatek, and D. Kaczorowski, Interplay of atomic randomness and Kondo effect in disordered metallic conductor La_2NiSi_3, J. Phys.: Condens. Matter **28**, 435602 (2016).
[44] D. Gnida, Electronic Griffiths phase and quantum interference in disordered heavy-fermion systems, Phys. Rev. B **97**, 081112(R) (2018).
[45] P. A. Lee and T. V. Ramakrishnan, Disordered electronic systems, Rev. Mod. Phys. **57**, 287 (1985).
[46] R. N. Bhatt, P. Wölfle, and T. V. Ramakrishnan, Localization and interaction effects in anisotropic disordered electronic systems, Phys. Rev. B **32**, 569 (1985).
[47] P. Wölfle and R. N. Bhatt, Electron localization in anisotropic systems, Phys. Rev. B **30**, 3542 (1984).
[48] A. Kawabata, Theory of negative magnetoresistance in three-dimensional systems, Solid State Commun. **34**, 431 (1980).
[49] A. Schmid, On the dynamics of electrons in an impure metal, Z. Phys. **271**, 251 (1974).
[50] A. Sergeev and V. Mitin, Electron-phonon interaction in disordered conductors: Static and vibrating scattering potentials, Phys. Rev. B **61**, 6041 (2000).
[51] J. J. Lin and J. P. Bird, Recent experimental studies of electron dephasing in metal and semiconductor mesoscopic structures, J. Phys.: Condens. Matter **14**, R501 (2002).

[52] P. Mohanty, E. M. Q. Jariwala, and R. A. Webb, Intrinsic decoherence in mesoscopic systems, Phys. Rev. Lett. **78**, 3366 (1997).

[53] J. J. Lin, Y. L. Zhong, and T. J. Li, Effect of annealing on electron dephasing in three-dimensional polycrystalline metals, Europhys. Lett. **57**, 872 (2002).

[54] N. Kumar, D. V. Baxter, R. Richter, and J. O. Strom-Olsen, Weak localization in two and three dimensions: Dephasing by zero-point motion, Phys. Rev. Lett. **59**, 1853 (1987).

[55] B. Altshuler, M. Gershenson, and I. Aleiner, Phase relaxation of electrons in disordered conductors, Physica E **3**, 58 (1998).

[56] S. M. Huang, T. C. Lee, H. Akimoto, K. Kono, and J. J. Lin, Observation of strong electron dephasing in highly disordered $Cu_{93}Ge_4Au_3$ thin films, Phys. Rev. Lett. **99**, 046601 (2007).

[57] J. J. Lin and N. Giordano, Electron scattering times from weak localization studies of Au-Pd films, Phys. Rev. B **35**, 1071 (1987).

[58] J. Reindl, H. Volker, N. P. Breznay, and M. Wuttig, Persistence of spin memory in a crystalline, insulating phase-change material, npj Quantum Mater. **4**, 57 (2019).

[59] H. Fukuyama and K. Hoshino, Effect of spin-orbit interaction on magnetoresistance in the weakly localized regime of three-dimensional disordered systems, J. Phys. Soc. Jpn. **50**, 2131 (1981).